Physics in Medicine and Biology

IPEM Institute of Physics and Engineering in Medicine

ACCEPTED MANUSCRIPT

A CBCT study of the gravity-induced movement in rotating rabbits

To cite this article before publication: Jeffrey Barber *et al* 2018 *Phys. Med. Biol.* in press https://doi.org/10.1088/1361-6560/aabf12

A CBCT study of the gravity-induced movement in rotating rabbits

Jeffrey Barber[1,2], Chun-Chien Shieh[3], William Counter[3], Jonathan Sykes[1,2], Peter Bennett[3], Verity Ahern[4], Stéphanie Corde[5], Soo-Min Heng[5], Paul White[5], Michael Jackson[5], Paul Liu[3], Paul J Keall[3,6], Ilana Feain[3,6]

1 Blacktown Cancer & Haematology Centre, Blacktown Hospital, NSW 2148, Australia
2 School of Physics, University of Sydney, NSW 2006, Australia
3 ACRF Image-X Institute, Sydney Medical School, University of Sydney, NSW 2006, Australia
4 Crown Princess Mary Cancer Centre, Westmead Hospital, NSW 2145, Australia
5 Nelune Comprehensive Cancer Centre, Prince of Wales Hospital, NSW 2031, Australia
6 Leo Cancer Care, Eveleigh, NSW 2015, Australia

Abstract

Fixed-beam radiotherapy systems with subjects rotating about a longitudinal (horizontal) axis are subject to gravity-induced motion. Limited reports on the degree of this motion, and any deformation, has been reported previously. The purpose of this study is to quantify the degree of anatomical motion caused by rotating a subject around a longitudinal axis, using cone-beam CT (CBCT).

In the current study, a purpose-made longitudinal rotating was aligned to a Varian TrueBeam kV imaging system. CBCT images of three live rabbits were acquired at fixed rotational offsets of the cradle. Rigid and deformable image registrations back to the original position were used to quantify the motion experienced by the subjects under rotation.

In the rotation offset CBCTs, the mean magnitude of rigid translations was 5.7 ± 2.7 mm across all rabbits and all rotations. The translation motion was reproducible between multiple rotations within 2.1 mm, 1.1 mm, and 2.8 mm difference for rabbit 1, 2, and 3, respectively. The magnitude of the mean and absolute maximum deformation vectors were 0.2 ± 0.1 mm and 5.4 ± 2.0 mm respectively, indicating small residual deformations after rigid registration. In the non-rotated rabbit 4DCBCT, respiratory diaphragm motion up to 5 mm was observed, and the variation in respiratory motion as measured from a series of 4DCBCT scans acquired at each rotation position was small.

The principle motion of the rotated subjects was rigid translational motion. The deformation of the anatomy under rotation was found to be similar in scale to normal respiratory motion. This indicates imaging and treatment of rotated subjects with fixed-beam systems can use rigid registration as the primary mode of motion estimation. While the scaling of deformation from rabbits to humans is uncertain, these proof-of-principle results indicate promise for fixed-beam treatment systems.

1. Introduction

The standard approach to radiotherapy has been for the imaging and treatment beams to be on a gantry rotating about a patient receiving treatment on a fixed couch. Fixed-beam systems would lower the cost of particle therapy (Burns and Potts 1992, Pankuch 2015), MRI-guided and economical photon linacs (Eslick and Keall 2015, Feain *et al* 2016, 2017b). However, patient rotation would be required to provide multi-field and arc deliveries equivalent to modern treatment deliveries on rotating gantry equipment (image-guided modulated treatments with passive respiratory motion management).

Image-guided small animal irradiator prototypes have been used with fixed kV sources and rotating subject stages, with the animal cranial-caudal axis placed vertically (Wong *et al* 2008, Matinfar *et al* 2009). To scale up to human treatments, the vertical patient orientation would have limited applications due to restricted beam geometry when seated or inability to maintain an upright weight bearing position over treatment. For a fixed-beam treatment system that could be used on all patients, the ideal configuration would be to have the patient lay down and rotate on a longitudinal axis, as this allows beam paths to most anatomy and would match standard simulation CT images and experience. Longitudinal rotation would introduce anatomic structure movement of the patient due to gravity as the couch support system rotates, which is a challenge for accurately conforming the treatment beam to the desired targets and minimising healthy tissue irradiation.

This investigation was performed to determine the feasibility of treatment units with fixed-beam and longitudinal subject rotation. Such a system would need to account for any motion created by subject rotation, in both treatment and image guidance systems. Modelling gravity effects on the pose of an external structure is a prominent issue in computer vision, incorporating articulated body pose estimation and pose space deformation (Lewis *et al* 2000). However, to date there has been little work to assess internal anatomical deformation.

The purpose of this study is to quantify the degree of anatomical motion caused by rotating a subject around a longitudinal axis, using cone-beam CT (CBCT). Respiration is the main source of motion in a non-rotated patient, and the gravity-induced deformation is compared to nominal respiratory deformation of the subject using 4DCBCT. This is the first study of CBCT imaging of live subjects undergoing gravity-induced motion, and as such it is piloted on small animals.

2. Methods

2.1 Image Acquisition

A purpose-built rotating immobilization cradle was positioned on the couch system at isocentre of a Varian TrueBeam linac v2.5 (Varian Medical Systems, Palo Alto CA), and its longitudinal rotation axis aligned to rotational axis of the gantry. This cradle acts as a simplified miniature of the couch in Feain *et al* 2017a. CBCT images of the cradle at fixed rotation offset increments were used to ensure the alignment and concentricity of the cradle and the linac imaging system.

In an institution ethics committee approved study (University of Sydney Animal Ethics Project 2015/903), three New Zealand white rabbits of 12-16 weeks (weighing 351, 359g and 406g; caudal-cranial lengths approximately 22cm) were imaged under free-breathing. Rabbits were placed in the cradle in the standard anatomical position (see FIGURE 1 and FIGURE 2). The rabbits were immobilised in the rotation cradle using adjustable straps, packed with bubble-wrap and secured in a wrapped towel. The cradle allowed 360° positioning under computer control. A veterinary surgeon anaesthetised each animal prior to imaging, and monitored them throughout the experiment.

Each rabbit was imaged with the following standard series: (1) An initial slow CBCT for 4DCBCT reconstruction with the cradle level and rabbit in standard anatomical position ("zero increment"). Images were based on the Head pre-set, with reduced gantry speed; (2) A series of standard CBCT (standard Head pre-set) with rotating gantry were acquired with the cradle rotated to a fixed position (this position will be referred to as the "fixed increment", and typically increment by 45° between image series). This was repeated over two full revolutions of the cradle, resulting in 16 CBCT. Additional series were acquired during another revolution which varied for each subject. These were: test of reproducibility and repeated rotations (rabbit 1), assessing gravity-induced changes to respiratory motion (rabbit 2) and assessing gravity-induced motion with finer resolution using smaller fixed-increment size (rabbit 3). The complete imaging schedule is detailed in TABLE 1. Continuous fluoroscopy with a fixed gantry position and constantly rotating cradle was acquired for a complementary project looking at reconstruction incorporating gravity-induced deformations (Shieh *et al* 2017). The settings for each acquisition are given in TABLE 2. All reconstructions used standard settings for the Head pre-set.

2.2 Registration Analysis

All CBCT were reconstructed on the TrueBeam system and imported to VelocityAI 3.2 (Varian Medical Systems, Palo Alto CA) for analysis. For each image, the fixed-increment rotation was registered back to the previous zero increment image. After each complete rotation (subject returns to zero), the image was registered back to the initial image for that rabbit, to assess reproducibility across subsequent revolutions.

For each CBCT, three image registrations were performed sequentially: (i) a manual rigid registration of the cradle was performed to remove the known applied cradle rotation offset from further registration results (e.g., to place all images in the same frame of reference). It was also used to determine the actual rotated position against the intended applied rotation on the cradle and hence the accuracy of the applied cradle rotation, and to verify concentricity of the rotation; (ii) A 6DoF rigid image registration (RIR) was performed using a mix of automatic and manual alignment to bony anatomy of the overall subject's thorax. This was a global registration, to account for movement within the external envelop formed by the immobilisation and not to account for any soft tissue differences. Where rigid alignment was difficult due to bony anatomy changing between two images (e.g., vertebral column flexion), priority in registration was given to vertebrae, ribs and chest wall, in that order; (iii) Deformable image registration (DIR) was performed using the rigid registration as a starting point. B-spline registration was run using the finest spline resolution available (5 mm), applied to a bounding box covering the whole thorax. The DIR was used to quantify all non-rigid body movement (between parts of the bony anatomy, and both within soft tissue organs and the external skin contour).

The rigid translation vectors were extracted for assessment of global translations, while the deformation vector field (DVF) was exported for the DIR. A histogram of the DVF was extracted for assessment of the localised deformation.

2.3 Respiratory motion

For each 4DCBCT at the zero-increment position, the respiratory motion was characterised by tracking the most superior position of the diaphragm in each phase-bin set, and a spline fit was generated. This was also performed for the 4DCBCT of rabbit 2 with cradle rotation.

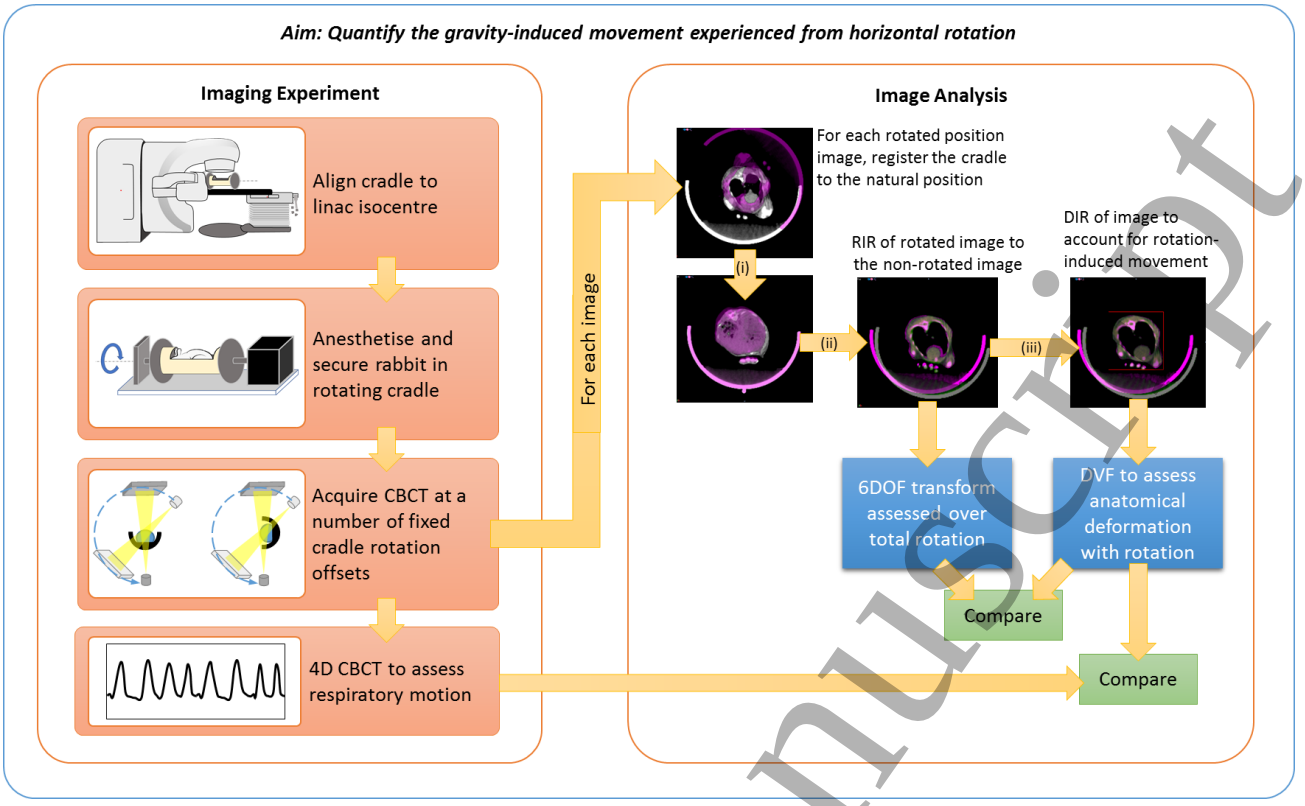

Figure 1 – Study design overview. The cradle in the zero offset (non-rotated) position. Rabbits were placed within the tube cutaway, and secured with adjustable straps and bubble-wrap packing (not shown). CBCT were then acquired at fixed rotation offset increments over a full revolution. All images were registered with both rigid and deformable methods to the zero offset position, to quantify movement due to the applied rotations. RIR = Rigid Image Registration. DIR = Deformable Image Registration.

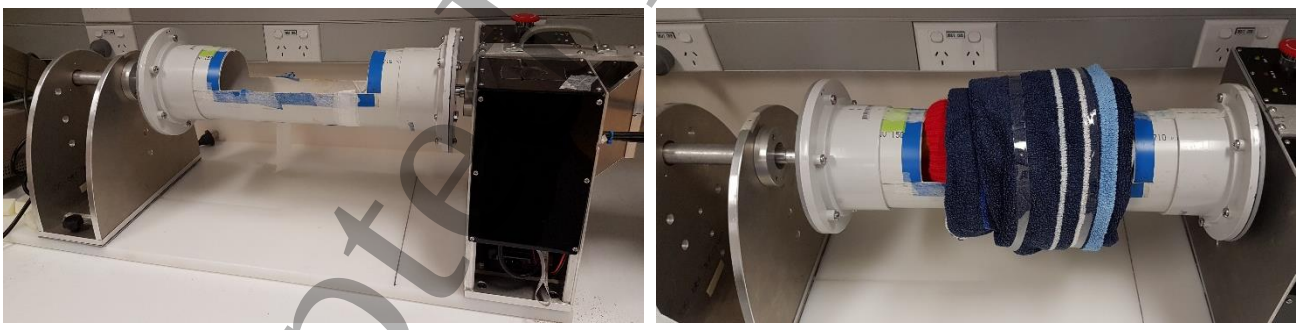

Figure 2 – Left picture shows rotation cradle with cutaway section for securing the subject, which resides on a flat wax base inside the tube cradle. Motor and computer control for rotation is in rear. Right is a mock-up immobilisation of a subject. The cutaway section is packed with bubble wrap, and secured around the subject with towel padding, ensuring adequate ventilation.

Table 1 – Imaging sequence across the subjects. Each subject received a different set of images during the second cradle revolution. All rabbits received each imaging set in the table, except for Imaging Revolution 2 where the set varied between animals as described. 0° refers to the cradle in its normal position.

Imaging Sets	**#scans**	**Cradle Rotation Increments**
Slow CBCT	1	0°
CBCT Revolution 1	8	0° – 315°, in 45° increments
CBCT Revolution 2 *, **, ***	8	0° – 315°, in 45° increments
Fluoroscopy (fixed gantry, rotating subject)	2	Continuously rotating

*Rabbit 1 underwent this series of images twice

**Rabbit 2 scanned with slow CBCT pre-set for this series

***Rabbit 3 scanned at 15° offset increments for this series

Table 2 – Image acquisition settings

Scan Type	**kV**	**mAs**	**Projections/s**	**Acquisition time (s)**	**Angle range (°)**	**Rotation speed (°/s)**
Standard CBCT	100	148	15	33	200	6
Slow CBCT	100	594	15	132	200	1.5
Fluoroscopy	100	0.3	15	120	360	3*

*Only the cradle rotated for fluoroscopy mode, while only the x-ray imager rotated during the CBCT modes.

Table 3 – The mean (and maximum) components from all the fixed increment registrations (mean of absolute values). Roll is reported as the mean difference from the nominal fixed offset roll averaged across all images. Translations and rotations are in units of mm and degrees, respectively.

Registration mean (maximum)	**Rabbit 1**	**Rabbit 2**	**Rabbit 3**
3D magnitude translation (mm)	3.9 (7.2)	4.6 (7.3)	6.7 (11.3)
LR translation (mm)	2.6 (7.0)	2.8 (5.4)	4.9 (9.6)
AP translation (mm)	2.1 (5.4)	2.8 (5.3)	2.6 (6.7)
CC translation (mm)	1.1 (2.1)	0.9 (1.9)	2.4 (5.3)
Pitch (°)	1.9 (5.5)	0.8 (2.5)	2.1 (7.8)
Yaw (°)	1.2 (5.8)	1.0 (2.1)	0.8 (3.3)
Roll (°)	5.3 (9.0)	3.9 (5.9)	6.2 (14.3)
Deformation (mm)	0.2 (0.4)	0.2 (0.3)	0.3 (0.5)

3. Results:

The rotation cradle was aligned to the linac imaging isocentre within <0.5 mm using a series of CBCT images at different rotation points, and the computer controlled fixed increments of rotation were verified to be accurate with a mean deviation of 0.2° based on image registration of the cradle itself. All rabbits were successfully imaged during the anaesthetic time frame, and all planned images were collected. FIGURE 3 shows example slices from each CBCT in a revolution series for one rabbit.

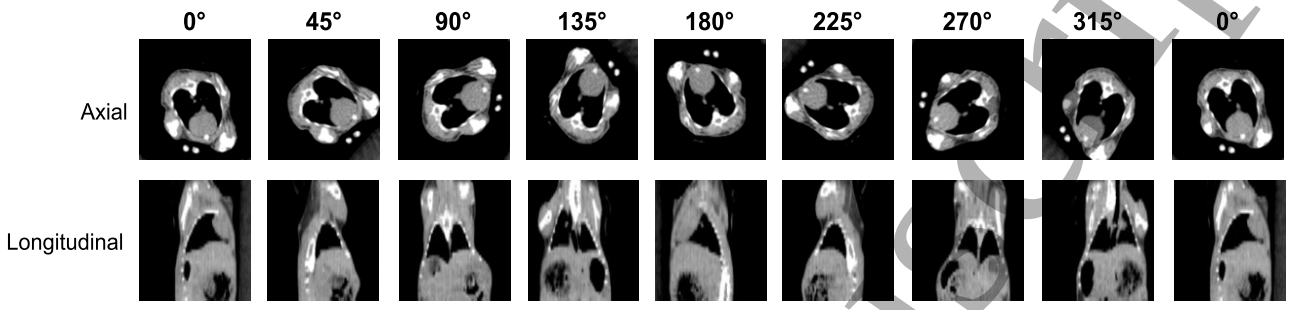

Figure 3 – An example of the CBCT acquired at each cradle rotation offset for a full revolution of rabbit 1. Transverse plane views through thorax on top row and vertical plane views on bottom row.

3.1 Rigid component of gravity-induced motion

The mean 3D magnitude of rigid registrations of the subjects was 5.7 ± 2.7 mm across all rabbits and revolutions. The absolute mean and maximum of each component of the registration is shown in TABLE 3. FIGURE 4 shows the rigid registrations for all images, mapped over cradle rotation offset angle and for each translation component. This figure also demonstrates the reproducibility of rigid motion between revolutions as well as between subjects. Note the second revolution for rabbit 3 deviated more than the others as it moved within the immobilisation.

The translational motion was reproducible for multiple rotations, within 2.1 mm, 1.1 mm, and 2.8 mm difference for rabbit 1, 2, and 3, respectively. Rabbit 3 was imaged with the finer 15° cradle rotation increments, however the trend in rigid registration followed the coarser 45° increment, indicating this is sufficient resolution.

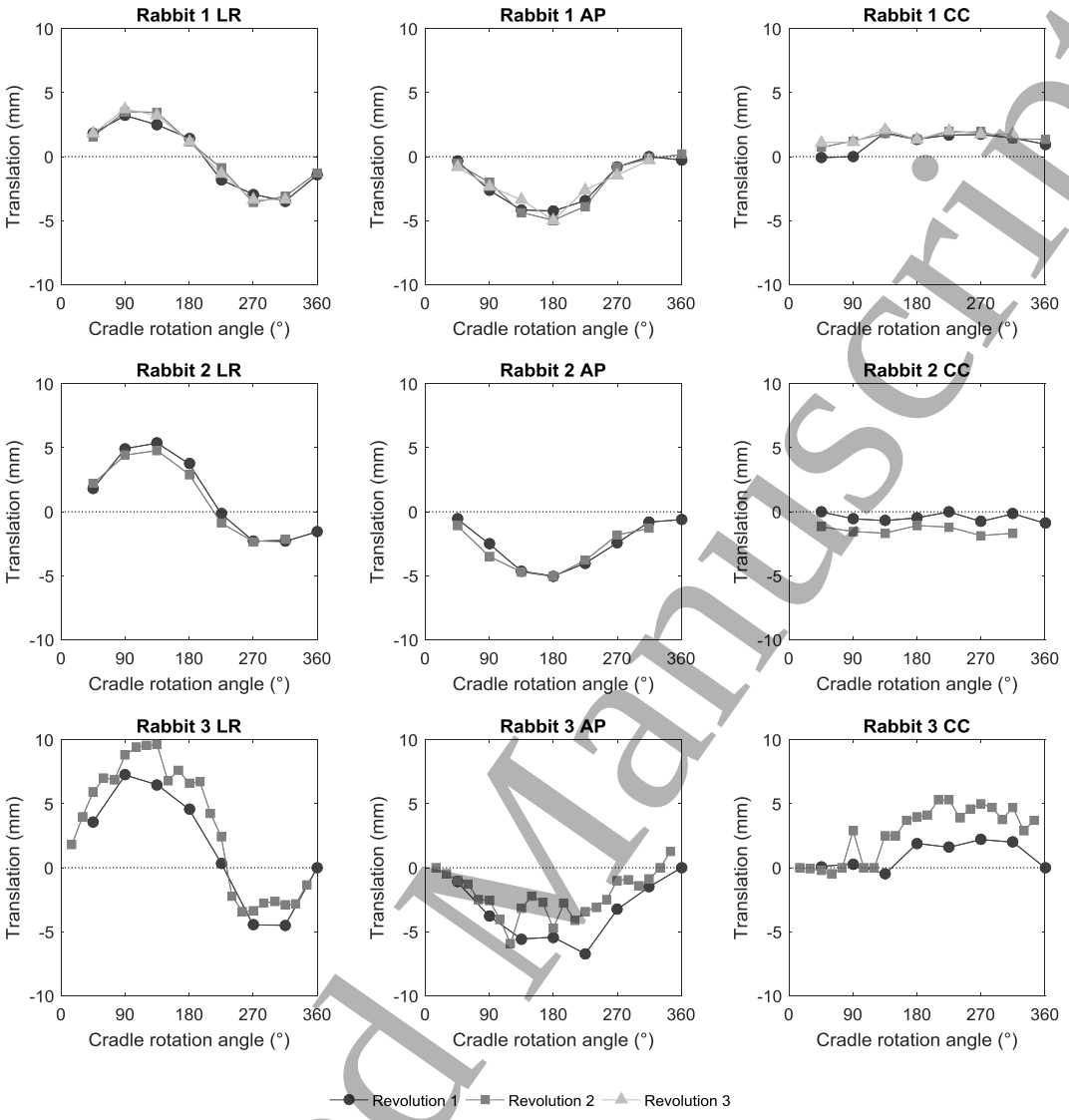

Figure 4. The translation magnitude of the rigid registrations as a function of rotation angle. The main motion is translation in the axial planes, with minimal changes cranial-caudal. The mean magnitude of rigid registrations was 5.7 ± 2.7 mm across all rabbits and rotations. Subject rotation was shown to be reproducible over cradle multiple rotations (shown by multiple lines for each rabbit).

3.2 Deformation component of gravity-induced motion

Residual thorax deformations were smaller than initial translational motion (TABLE 3). Vector direction was qualitatively verified to ensure the registration was physical and realistic. A normalised cumulative histogram of the DVF magnitude was then generated (see FIGURE 5). The 50th and 95th percentile for each histogram was also extracted, where the 50th percentile indicates the median deformation and the 95th percentile is reported to indicate maximum deformations (avoiding spurious results in the DIR where surface elements were stretched to non-physical results).

The mean DVF magnitude for all 50th percentiles was 1.2 mm (standard deviation 0.4; range [0.5, 2.5]) and for 95th percentiles was 2.6 mm (standard deviation 0.7; range [1.0, 5.2]). Each rabbit exhibited a different trend in maximum deformation vectors with rotation – rabbit 1 exhibited the clearest trend, peaking near 225°, after inversion; rabbit 2 peaked near 90°, prior to inversion, with most movement being lateral; rabbit 3 had less of a clear trend due to large lateral movement not observed in the other rabbits (due to the subject being less secure in the cradle), and maximum deformation was seen near 315° as it returned back to the zero cradle offset position.

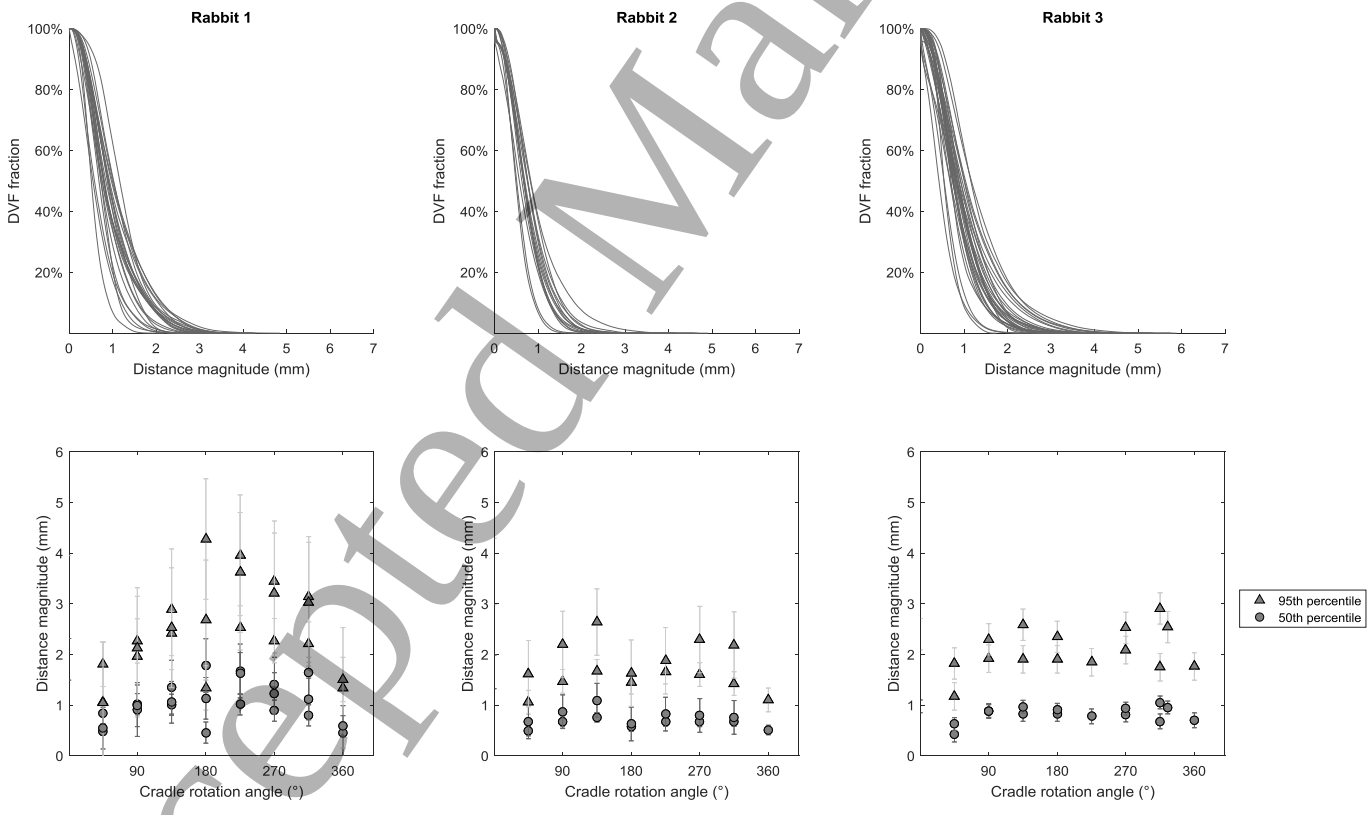

Figure 5. Cumulative histograms of thorax DVF magnitude (top row). Residual deformation is obtained after removing the translational registration above. All rotated images for each rabbit are shown (85 plots total). The deformations observed were smaller than the translational motion. The 95th-percentile of each DVF displayed a small dependency on cradle rotation angle (bottom row).

3.3 Comparison of gravity-induced motion to respiratory motion

In the non-rotated rabbit 4DCBCT, respiratory diaphragm motion of 2 – 5 mm was observed (FIGURE 6). This was of a similar magnitude to the total mean 3D gravity-induced translations (5.7 ± 2.7 mm), and larger than the deformation vectors (mean and absolute maximum 0.2 ± 0.1 mm and 5.4 ± 2.0 mm respectively).

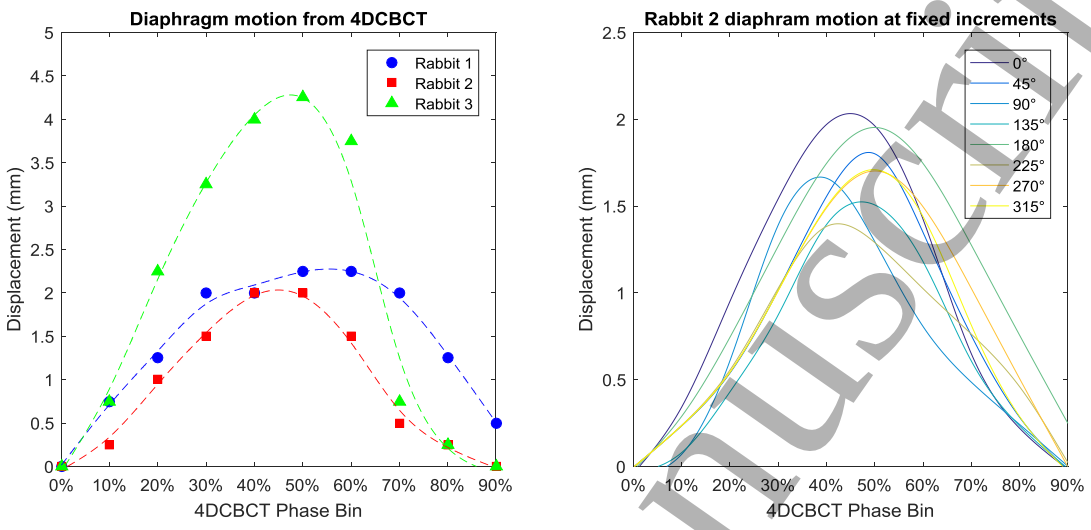

Figure 6. (a) Respiratory motion of the rabbits without rotation, as observed using diaphragm cranial-caudal motion. (b) Rabbit 2 4DCBCT diaphragm motion for each cradle rotation offset.

Additional imaging of rabbit 2 for 4DCBCT acquired at fixed 45 increments showed the respiratory motion had amplitudes in the range 1.5 – 2 mm and did not exhibit a clear trend with subject rotation (FIGURE 6(b)). The segmented lung volume and surface area with rotation angle on the 3D CBCT also did not have any clear trend with rotation, but did vary up to 8% and 15% respectively across the rotated offset scans.

4. Discussion:

In this paper, we rotated three rabbits and measured the gravity-induced motion with CBCT. Our results indicate that gravity-induced motion is primarily translational rather than rotational or deformation in small animals. In terms of magnitude, the translational/sliding motion of the animals was approximately 80% of the observed motion, and was highly reproducible for two of the three subjects. The gravity-induced deformations were of lower magnitude than normal respiration. It is still to be seen how the motion would scale with size and weight in the range of a human.

While the gravity-induced translations were large, these can be mitigated with purpose-designed, well-executed immobilisation systems. This is especially important for future studies in larger animals. A suitable patient rotation system has been designed for the fixed gantry Nano-X Tatum prototype, featuring pressure-controlled airbags and straps in addition to standard radiotherapy fixation devices (Feain *et al* 2017a). An MRI-compatible patient rotation system has also been designed and investigated (Whelan *et al* 2017).

A source of uncertainty in the results presented is the resolution of the CBCT and DVF. The images used in this work were reconstructed with the standard clinical CBCT voxel cranio-caudal dimension of 2mm. The cranial-caudal length of the rabbit lungs was 30-35 mm, which meant there was limited information in this dimension. However, the 4DCBCT images were reconstructed with isotropic 0.25 mm voxels to better quantify the small scale of diaphragm movement. Comparison of DIR with the higher and lower resolution reconstructions did not lead to significant changes in results.

The DIR algorithm used had a limitation of 5mm spline grid resolution. This was large compared to the lung dimensions, however the deformed images had good visual agreement, indicating this limitation helped to regularise the DIR and maintain realistic solutions. After DIR, residual mismatch in deformably registered images was measured up to 2-3mm in the thoracic region, and larger beyond (legs, spine flexion). This sets an inherent uncertainty to the DIR results, again indicating the role of immobilisation to fix the pose of subjects under rotation.

While it is difficult to generalise these results to larger subjects, small animal models provide a means of acquiring information that is not achievable with human subjects. It is a common limitation in radiotherapy that a human subject cannot be imaged at the frequency used in this study. A preliminary human experiment using a different imaging modality indicates deformations of a similar order of magnitude (Whelan *et al* 2017). In that study, for MR pelvic imaging of a study of a single volunteer human under a single rotation, the prostate, bladder and rectum showed a mean rigid displacement of structure surfaces by 3 – 6 mm, and mean organ surface deformation of 1 – 3 mm.

To date there are no other published studies to the authors knowledge that investigate internal anatomy deformations under gravity induced rotation with x-ray imaging. While prototype small animal irradiators envisaged fixed sources and rotation stages rotate about a vertical axis, which negates the impact of gravity induced motion (Matinfar *et al* 2009), the commercial units have horizontal subject stages and rotating x-ray gantries (Xstrahl Medical & Life Sciences 2015, PXi Precision X-ray 2015). Vertical CT (Shah *et al* 2009) and seated fixed-beam treatments (Pankuch 2015, McCarroll *et al* 2017) are under development. Many cancer patients would be unable to maintain an immobilised upright or seated stance such as this over the course of radiotherapy treatment, or it may be undesirable as it limits the available beam entry paths to treatment areas. As the scientific and technical challenges are addressed, a longitudinal rotation patient support system could provide a singular solution to a fixed gantry radiotherapy delivery system.

We are advancing these pre-clinical results to clinical applications through two separate studies. We have ethics approval to perform a 100-patient study of their experience in a novel radiotherapy patient rotation system described in Feain *et al* 2017a. We are in the process of obtaining ethics approval for a 30-patient study that, in addition to measuring the patient experience under rotation, will also acquire volumetric MRI imaging data. This imaging data will be used to quantify human anatomic deformation due to gravity and also the impact on treatment planning. The latter study will use the MRI-compatible patient rotation system described by Whelan *et al* 2017.

5. Conclusion:

This novel study investigates gravity-induced motion from longitudinal rotation on live animal subjects. The results of this imaging study showed that deformations introduced by subject rotation were of the same magnitude as physiological motion from respiration. The proof-of-principle is shown in rabbits, with encouraging results showing promise for larger subjects. By collecting images at fixed rotation points, we collected a ground truth for further work to develop methods for CBCT reconstruction incorporating motion with fixed source and rotating subject.

The principle motion of the rotated subjects was translational due to movement of internal tissues inside the animal. The deformation of the anatomy under rotation was found to be equal in scale to normal physiological motion. This indicates imaging and treatment of rotated subjects with fixed-beam systems can use rigid registration as the primary mode of motion estimation. While the scaling of deformation from rabbits to humans is uncertain, these proof-of-principle results indicate promise for fixed-beam treatment systems, implying it may be possible to do image-guided radiotherapy with fixed-beam systems and achieve similar accuracy to that practiced in the current standard of care for lung cancer radiotherapy, i.e. image guidance based on respiratory-blurred CBCT scans.

Acknowledgements

The authors acknowledge the support of staff at Nelune Cancer Centre (Prince of Wales Hospital, Sydney) and Crown Princess Mary Cancer Centre (Westmead Hospital, Sydney) for this work. Partially funded by NHMRC Development Grant APP1118450.

Conflict of Interest

Authors Feain and Keall are shareholders and directors of Nano-X Pty. Ltd., a radiation therapy machine which incorporates patient rotation. Authors Feain and Keall are inventors on several pending patents involving patient rotation during radiotherapy.

References

Burns C A and Potts A 1992 Design of a patient restraint system *Applied Ergonomics* vol 23(Interrface '91, Proc Seventh Symp on Human Factors and Industrial Design in Consumer Products, Dayton, Ohio.)p 287 Online: https://doi.org/10.1016/0003-6870(92)90192-X

Eslick E M and Keall P J 2015 The Nano-X Linear Accelerator *Technol. Cancer Res. Treat.* **14** 565–72 Online: http://journals.sagepub.com/doi/10.7785/tcrt.2012.500436

Feain I, Coleman L, Wallis H, Sokolov R, O'Brien R, Keall P, Brien R O, Keall P, Feain I, Coleman L, Wallis H, Sokolov R, O'Brien R and Keall P 2017a Technical Note: The Design and Function of a Horizontal Patient Rotation System for the Purposes of Fixed-Beam Cancer Radiotherapy *Med. Phys.* Online: http://doi.wiley.com/10.1002/mp.12219

Feain I, Court L, Palta J, Beddar S and Keall P 2017b Innovations in Radiotherapy Technology *Clin. Oncol.* **29** 120–8 Online: http://dx.doi.org/10.1016/j.clon.2016.10.009

Feain I, Shieh C C, White P, O'Brien R, Fisher S, Counter W, Lazarakis P, Stewart D, Downes S, Jackson M, Baxi S, Whelan B, Makhija K, Huang C Y, Barton M and Keall P 2016 Functional imaging equivalence and proof of concept for image-guided adaptive radiotherapy with fixed gantry and rotating couch *Adv. Radiat. Oncol.* **1** 365–72 Online: http://dx.doi.org/10.1016/j.adro.2016.10.004

Lewis J P, Cordner M and Fong N 2000 Pose Space Deformation : A Unified Approach to Shape Interpolation and Skeleton-Driven Deformation *Proc. 27th Annu. Conf. Comput. Graph. Interact. Tech. - SIGGRAPH '00* 165–72 Online: http://portal.acm.org/citation.cfm?doid=344779.344862

Matinfar M, Ford E, Iordachita I, Wong J and Kazanzides P 2009 Image-guided small animal radiation research platform: calibration of treatment beam alignment. *Phys. Med. Biol.* **54** 891–905 Online: http://www.pubmedcentral.nih.gov/articlerender.fcgi?artid=2964666&tool=pmcentrez&rendertype=abstract

McCarroll R E, Beadle B M, Fullen D, Balter P A, Followill D S, Stingo F C, Yang J and Court L E 2017 Reproducibility of patient setup in the seated treatment position: A novel treatment chair design *J. Appl. Clin. Med. Phys.* **18** 223–9

Pankuch M 2015 Horizontal Plane Computed Tomography CT's in the seated position *AAPM Midwest Spring Meeting* Online: http://chapter.aapm.org/midwest/2015SpringMeeting/Pankuch_Horizontal_Plane_Scanner.pdf

PXi Precision X-ray 2015 X-RAD SmART, Small Animal Image Guided Irradiation System Online: http://www.pxinc.com/products/small-animal-igrt-platform/x-rad-smart-small-animal-radiation-therapy-precision-xray-branford-connecticut/

Shah A P, Strauss J B, Kirk M C, Chen S S, Kroc T K and Zusag T W 2009 Upright 3D Treatment Planning Using a Vertical CT *Med. Dosim.* **34** 82–6

Shieh C, Barber J, Counter W, Sykes J, Bennett P, Heng S, White P, Corde S, Jackson M, Ahern V, Keall P and Feain I 2017 SU-F-201-1 Cone-beam CT reconstruction with gravity- induced motion *Med. Phys.* **44**

2758 Online: http://www.aapm.org/meetings/2017AM/PRAbs.asp?mid=127&aid=35847

Whelan B, Liney G P, Dowling J A, Rai R, Holloway L, McGarvie L, Feain I, Barton M, Berry M, Wilkins R and Keall P 2017 An MRI-compatible patient rotation system - Design, construction, and first organ deformation results: *Med. Phys.* **44** 581–8

Wong J, Armour E, Kazanzides P, Iordachita I, Tryggestad E, Deng H, Matinfar M, Kennedy C, Liu Z, Chan T, Gray O, Verhaegen F, McNutt T, Ford E and DeWeese T L 2008 High-Resolution, Small Animal Radiation Research Platform With X-Ray Tomographic Guidance Capabilities *Int. J. Radiat. Oncol. Biol. Phys.* **71** 1591–9

Xstrahl Medical & Life Sciences 2015 SARRP Small Animal Radiation Research Platform Online: https://xstrahl.com/life-science-systems/small-animal-radiation-research-platform/